

THE VARIABLE QUIESCEENCE OF CEN X-4

S. CAMPANA¹, G.L. ISRAEL², L. STELLA², F. GASTALDELLO³, S. MEREGHETTI³
Draft version December 3, 2018

ABSTRACT

Cen X-4 is one of the best studied low-mass neutron star transients in quiescence. Thanks to XMM-Newton large throughput, Cen X-4 was observed at the highest signal to noise ever. This allowed us to disclose rapid (> 100 s), large (45 ± 7 rms in the $10^{-4} - 1$ Hz range) intensity variability, especially at low energies. In order to highlight the cause of this variability, we divided the data into intensity intervals and fit the resulting spectra with the canonical model for neutron star transients in quiescence, i.e. an absorbed power law plus a neutron star atmosphere. The fit is consistent with a variable column density plus variability in (at least) one of the spectral models. Variations in the neutron star atmosphere might suggest that accretion onto the neutron star surface is occurring in quiescence; variations in the power law tail should support the view of an active millisecond radio pulsar emitting X-rays at the shock between a radio pulsar wind and inflowing matter from the companion star.

Subject headings: accretion, accretion disks — binaries: close — star: individual (Cen X-4) — stars: neutron

1. INTRODUCTION

Many Low Mass X-ray Binaries (LMXRB) accrete matter at very high rates, and therefore shine as bright X-ray sources, only sporadically. Among these systems are Soft X-ray Transients (SXRTs) hosting an old neutron star (for a review see Campana et al. 1998a). These systems alternate periods (weeks to months) of high X-ray luminosity, during which they share the same properties of persistent LMXRBs, to long (1–few 10 years) intervals of quiescence in which the X-ray luminosity drops by up to 5–6 orders of magnitude.

Cen X-4 is one of the best studied SXRTs. Bright X-ray outbursts were detected in 1969 and 1979; the source remained quiescent since. During the 1979 outburst Cen X-4 reached a peak flux $L_X \sim 4 \times 10^{37}$ erg s $^{-1}$ (for a distance of $d \sim 1.2$ kpc, Kaluzienski, Holt & Swank 1980). Type I bursts were observed, testifying to the presence of an accreting neutron star. Cen X-4 was observed several times in quiescence (Asai et al. 1996, 1998; Campana et al. 1997, 2000; Rutledge et al. 2001). The spectrum was fit with a soft thermal component (neutron star atmosphere or black body) plus a hard power law with photon index in the 1–2 range. Rutledge et al. (2001) reported that the 0.5–10 keV luminosity decreased by $40 \pm 8\%$ in the 5 yr between the ASCA and Chandra observations. This variability can be attributed to the power-law component; on the contrary temperature variations in the thermal component are limited to $\lesssim 10\%$. Short time variability was discovered by Campana et al. (1997) during a ROSAT HRI pointing, with the source flux fading by a factor of ~ 3 on a timescale of $\lesssim 4$ days.

Extensive spectroscopic and photometric measurements of the optical counterpart in quiescence ($V=18.7$ mag) led to the determination of the orbital period (15.1 hr; Chevalier et al. 1989; McClintock & Remillard 1990; Cowley et al. 1988) and mass function ($\sim 0.2 M_\odot$, converting to a neutron star mass between $0.5 - 2.3 M_\odot$). The op-

tical spectrum shows the characteristics of a K5–7 main sequence star, contaminated by lines (e.g. H α , H β and H γ) and continuum emission probably resulting from an accretion disk (Shahbaz, Naylor & Charles 1993). The latter was estimated to contribute $\sim 80\%$, $\sim 30\%$, $\sim 25\%$ and $\sim 10\%$ of the quiescent optical flux in the B, V, R and I bands, respectively. A short wavelength HST/FOS spectrum of the quiescent optical counterpart yielded a 1350–2200 Å luminosity of $0.6 - 4 \times 10^{31}$ erg s $^{-1}$. These results were confirmed by higher quality HST/STIS spectra (McClintock & Remillard 2000). In particular, the UV spectrum appears to lie on the extrapolation of the power law component seen in X rays.

In this paper we take advantage of an XMM-Newton observation of Cen X-4 to investigate, in much higher detail its quiescent state. We describe the observation characteristics and data filtering in Section 2. In Section 3 we discuss on spectral and timing results. The interpretation of the data and discussion is presented in Section 4. Our conclusions are in Section 5.

2. OBSERVATION AND DATA ANALYSIS

The XMM-Newton Observatory (Jansen et al. 2001) comprises three ~ 1500 cm 2 effective area X-ray telescopes each with a European Photon Imaging Camera (EPIC, 0.1–15 keV) at the focus. Two of the EPIC imaging spectrometers use MOS CCDs (Turner et al. 2001) and one uses pn CCDs (Strüder et al. 2001). Reflection Grating Spectrometers (RGS, 0.35–2.5 keV, den Herder et al. 2001) are located behind two of the telescopes.

Cen X-4 was observed on 2001 August 20–21. The EPIC cameras were operated in the Prime Full Window mode with thin filters. We used the data generated by the Pipeline Processing Subsystem in September 2001. The observation is plagued by high background intervals due to soft proton flares. We excluded them using an intensity filter: all events accumulated in a time interval such

¹ INAF-Osservatorio Astronomico di Brera, Via Bianchi 46, I-23807 Merate (Lc), Italy

² INAF-Osservatorio Astronomico di Roma, Via Frascati 33, I-00040 Monteporzio Catone (Roma), Italy

³ CNR-IASF, Istituto di Astrofisica Spaziale e Fisica Cosmica Sezione di Milano “G.Occhialini”, Via Bassini 15, I-20133 Milano, Italy

that the rate, excluded the source region, exceeded 0.3 c s^{-1} in the 10–12 keV band for each of the two MOS cameras and 0.8 c s^{-1} for the pn camera were rejected. We adopted these thresholds, which are somewhat higher than the standard ones, motivated by the strength of our source ($\sim 1 \text{ c s}^{-1}$ in the 0.2–8 keV band of the pn, see below). We verified that results obtained by using standard thresholds are consistent with the cleaner (but shorter) exposures. We obtained net (original) exposure times of 32 (52) ks, 32 (52) ks, 24 (40) ks for MOS1, MOS2 and pn, respectively. These represent the deepest observation of a neutron star SXRT ever carried out. RGS spectra were heavily affected by soft proton flares due to the dispersion over the field of view. Optical monitor was not operated.

For the pn, single and double pixel events were selected (patterns 0 to 4), for the MOS, events corresponding to patterns from 0 to 12 were selected. Source spectra were extracted from a circular region of $45''$ for the two MOS cameras and $40''$ for pn camera, corresponding to an encircle energy fraction of $\sim 90\%$. Background spectra have been extracted from nearby circular regions $2'$ and $2.5'$ for the MOS1 and MOS2, respectively. For the pn we considered two circular regions of $40''$ and $60''$ in the same CCD of the source. Following the prescriptions of Snowden et al. (2002) we extracted the spectra (including the FLAG=0 option) obtaining 9609 counts (0.29 c s^{-1}), 9829 counts (0.30 c s^{-1}), 28673 counts (1.1 c s^{-1}) from the MOS1, MOS2 and pn in the full band, respectively. Note that pile up was negligible ($< 1\%$).

Response matrices and ancillary region files were generated with the SAS (v5.3.3) tasks `rmfgen` and `arfgen`. The spectral analysis was carried out in the 0.5–10 keV energy range for all the instruments using XSPEC (v11.2). All spectral uncertainties are given at 90% confidence level for one interesting parameter ($\Delta\chi^2 = 2.71$).

3. RESULTS

3.1. Spectral analysis: I

We first consider the total spectrum. We rebinned the MOS and pn spectra so as to have 25 and 30 counts per spectral channel, respectively. We verified that the background spectra, especially at high energies, are not dominated by residual soft proton flares. In particular, pn and MOS background spectra show the same behaviour and decrease by a factor of ~ 2 from 2 to 10 keV as expected for normal conditions (Lumb et al. 2002).

The spectrum cannot be fit with any single component model. We then tried the canonical spectrum for SXRT in quiescence (e.g. Campana et al. 1998b; Campana 2001), i.e. an absorbed neutron star hydrogen atmosphere plus a power law (we adopted the absorption model TBABS by Wilms, Allen & McCray 2000 and the neutron star atmosphere model by Gänsicke, Braje & Romani 2002). We included also a constant factor to account for the mismatch between the different EPIC instruments (Kirsch 2002). This model provides a reduced $\chi^2_{\text{red}} = 1.07$ for 518 degrees of freedom (d.o.f.), corresponding to a null hypothesis probability (n.h.p.) of 12% (see Fig. 1). Neutron star atmosphere models with iron or solar composition or a disk black body model provided worse fits with $\chi^2_{\text{red}} > 1.3$. A black body model formally provided a better fit to the data but with a null column density ($< 1.4 \times 10^{20} \text{ cm}^{-2}$ see

Table 1). Taking instead a column density of $9 \times 10^{20} \text{ cm}^{-2}$ (in line with expectations from optical data) we obtained a worse fit ($\chi^2_{\text{red}} = 1.18$).

The unabsorbed 0.5–10 keV flux of the power law plus neutron star atmosphere models is $2.3 \times 10^{-12} \text{ erg s}^{-1} \text{ cm}^{-2}$ that at a distance of 1.2 kpc translates into a luminosity of $3.9 \times 10^{32} \text{ erg s}^{-1}$. In the 0.5–10 keV band the atmosphere model accounts for 63% of the total luminosity.

3.2. Temporal analysis

For timing analysis we considered the entire observation, including high background time intervals. Besides source light curves, we extracted background light curves which we subtract (including the error on the background rate) from the source light curve. The resulting light curve is clearly not constant (Fig. 2). The importance of the background is in any case minimal apart from the minimum around 21.5 hr in Fig. 2 when the background reached 40% of the Cen X-4 rate.

We extracted light curves in selected energy bands: 0.2–1 keV, 1–2 keV and 2–8 keV (see Fig. 3). A smaller amplitude of the variability at high energies is apparent. Taking a bin time of 500 s (in order to have a mean of 30 counts per bin in the 2–8 keV light curve) we fit the light curves with a constant and we obtained $\chi^2_{\text{red}} = 13.7, 4.8, 1.6$ in the three energy bands, respectively. Possible flare-like events can be identified around 14 hr, 16.5 hr and 22.5 hr in Fig. 2. Rise times are about 20 min. A dip-like feature is also visible around 21.5 hr.

We obtained a power spectrum of the entire observation by using the cleanest pn exposure. The power spectrum shows a strong noise component below $\sim 0.01 \text{ Hz}$ (i.e. a timescale longer than $\sim 100 \text{ s}$), consistent with the variability discussed above. The rms variability amounts to $45 \pm 7\%$ in the $10^{-4} - 1 \text{ Hz}$ band. The power spectrum can be well fit with a power law with index -1.2 ± 0.1 . No significant periodicities or quasi-periodic oscillations are seen. The power-law index of the X-ray power spectrum is consistent with the optical one which is characterized by an index of $\sim -1, -1.5$ (Hynes et al. 2002; Zurita et al. 2003).

3.3. Spectral analysis: II

To study possible spectral changes related to the variability we constructed the color-color diagram made by a soft color (1–2 keV / 0.2–1 keV) versus a hard color (2–8 keV / 1–2 keV, see Fig. 4). Spectral variations are visible in the data. We plot in the same diagram the colors expected for single (absorbed) power law and neutron star atmosphere spectra for a set of parameters. As expected from the spectral analysis (section 3.1) these single component models cannot account for the data. In addition, we plot two lines with different column densities and different fractions of the two components models. We note that variations appear to be consistent with variations in the column density across the observation. Alternatively a variation in the fraction of the power law flux to neutron star atmosphere flux can account for the observed variation.

To check these hypotheses we carry out a more detailed spectral analysis. We concentrate on pn data, since these

provide a factor of ~ 2 more counts than the two MOS cameras together. We divided the data in the pn light curve (1,000 s bin) at three different count rates: above 1.3 c s^{-1} , between 1.0 and 1.3 c s^{-1} and below 1.0 c s^{-1} . We then fit the three corresponding spectra in order to search for possible differences. We consider the same absorbed power law plus neutron star atmosphere model. The same spectrum for the three count rate spectra is clearly not acceptable ($\chi^2_{\text{red}} = 2.60$). Letting the column density vary freely produces an improvement in the fit but not enough to make the fit acceptable ($\chi^2_{\text{red}} = 1.51$; the column density is smaller at larger count rates). This shows that the variability cannot be fully ascribed to a column density variation. Better results can be obtained allowing (at least) one of the spectral component to vary together with the column density⁴ (Table 2). With an additional parameter we obtained better results, however we cannot decide on a statistical basis which of the two fits is better. No clear correlations are observable. The column density is within the errors for both these new fits. In the case of a variable neutron star atmosphere, the temperature increases with the count rate, in the case of a variable power law, the power law photon index steepens as the count rate increases.

4. DISCUSSION

The quiescent state of Cen X-4 has been recognised to be variable both on long times scales ($\sim 40\%$ in 5 yr, Rutledge et al. 2001) and on shorter timescales (factor of ~ 3 in a few days, Campana et al. 1997). During this XMM-Newton observation X-ray variability has been observed (at a level of $\sim 45\%$ rms) on even shorter timescale (down to ~ 100 s) thanks to the large collecting area. Variability on such a short timescale would have been missed if observed with any previous X-ray satellite.

In the pn light curve three flare-like events can be identified. X-ray flares have been observed in the transient black hole candidate V404 Cyg also in quiescence (Wagner et al. 1994; Kong et al. 2002). Flare activity has been recently reported also in the optical for a number of transient black holes during quiescence as well as for Cen X-4 (Zurita, Casares & Shabhzad 2003; Hynes et al. 2002). Flares occur on timescales of minutes to a few hours, with no dependence on orbital phase. R-band luminosities are in the range $10^{31} - 10^{33} \text{ erg s}^{-1}$. The mean duration of optical flares in Cen X-4 is 21 min. This is similar to what observed in the X-rays.

Several mechanisms have been proposed for optical flares (Zurita et al. 2003; Hynes et al. 2002). Chromospheric activity, instabilities in the mass transfer rate from the companion and viscous instabilities in an accretion disk have been ruled out for different reasons (Zurita et al. 2003). Reprocessing of X-ray variations in the outer disk regions has also been considered less likely due to the

large ratio between optical and X-ray emission (Zurita et al. 2003). In passing, we note that in the X-ray light curve three flare events can be identified (see Fig. 2). The durations and energetics of the first two flares are comparable: 0.9 and 1.2 hr and 1.8 and 4.4×10^{35} erg, respectively. The last flare is much shorter and less energetic (0.1 hr and 0.6×10^{35} erg).

Long term X-ray variability in the quiescent state of Aql X-1 has also been reported based on Chandra data. In particular, Rutledge et al. (2002) showed that these variations cannot be caused by variations in the power law only, but can be accounted for by a varying temperature of the neutron star atmosphere model. These variations are not monotonic but show first a decrease, then an increase and finally a decrease in time. This would rule out the deep crustal heating mechanism for SXRTs in quiescence. Campana & Stella (2003) provided a different interpretation of these data (plus an additional BeppoSAX observations): a varying column density and power law component together with a stable neutron star atmosphere model.

This latter model is motivated by the recent discovery of a millisecond radio pulsar PSR J1740-5340 in the globular cluster NGC 6397 (D'Amico et al. 2001; Ferrario et al. 2001). This pulsar shows irregular eclipses in radio and it is also emitting in X-rays (Grindlay et al. 2001). The X-ray emission is likely powered by the interaction of the relativistic wind of the radio pulsar with matter outflowing from the companion. This shock emission mechanism has also been put forward to explain the X-ray emission of the radio pulsar PSR 1259-63 orbiting a Be companion (Tavani & Arons 1997). This model is not disproved by the data. The power law photon index is between 1.5 and 2 as one would expect from simple modelling based synchrotron emission. The luminosity increases as the power law photon index increases as observed in PSR 1259-63 for $\Gamma < 1.8$.

5. CONCLUSIONS

We observed large ($\sim 45\%$) r.m.s. X-ray variability in the quiescent state of Cen X-4. Small spectral variations are observed as well. These can be mainly accounted for by a variation in the column density together with another spectral parameter. Based on the available spectra we cannot prefer a variation of the power law versus a variation in the temperature of the atmosphere component (even if the first is slightly better in terms of reduced χ^2). This variability can be accounted for by accretion onto the neutron star surface (e.g. Rutledge et al. 2002) or by the variable interaction between the pulsar relativistic wind and matter outflowing from the companion in a shock front (e.g. Campana & Stella 2003).

We thank M. Guainazzi for his advice in the data analysis.

⁴ In the case of a free neutron star atmosphere component, we consider only a variation in temperature and check that indeed the neutron star radius remains stable.

REFERENCES

Asai, K., et al. 1996, PASJ 48 257
 Asai, K., et al. 1998, PASJ 50 611
 Campana, S. 2001, in the proceedings of the Bologna conference on "X-ray Astronomy 1999: Stellar Endpoints, AGN, and the Diffuse X-ray Background", eds. N.E. White, G. Malaguti, G.G.C. Palumbo, A.I.P. Conf. Proc. 599 63
 Campana, S., Stella, S. 2003, ApJ submitted
 Campana, S., et al. 1997, A&A 324 941
 Campana, S., et al. 1998a, A&A Rev. 8 279
 Campana, S., et al. 1998b, ApJ 499 L65
 Campana, S., et al. 2000, A&A 358 583
 Chevalier, C., Illovaiky, S.A., van Paradijs, J., Pedersen, H., van der Klis, M. 1989, A&A 210 114
 Cowley, A.P., Hutchings, J.B., Schmidtke, P.C., Hartwick, F.D.A., Crampton, D., Thompson, I.B. 1988, AJ 95 1231
 D'Amico, N., et al. 2001, ApJ 561 L89
 den Herder, J.W., et al. 2001, A&A 365 L7
 Ferrario, F., Possenti, A., D'Amico, N., Sabbi, E. 2001, ApJ 561 L93
 Gänsicke, B.T., Braje, T.M., Romani, R.W. 2002, A&A 386 1001
 Grindlay, J., Heinke, C.O., Edmonds, P.D., Murray, S.S., Cool, A.M. 2001, ApJ 563 L53
 Hynes, R. I., Zurita, C., Haswell, C. A., Casares, J., Charles, P. A., Pavlenko, E., Shugarov, S., & Lott, D. A. 2002, MNRAS 330 1009
 Jansen, F., et al. 2001, A&A 365 L1
 Kaluzienski L.J., Holt, S.S., Swank, J.H. 1980, ApJ 241 779
 Kong, A.K.H., McClintock, J.E., Garcia, M.R., Murray, S.S., Barret, D. 2002 ApJ 570 277
 Lumb, D.H., Warwick, R.S., Page, M., De Luca, A. 2002 A&A 389 93
 McClintock, J.E., Remillard, R.A. 1990, ApJ 350 386
 McClintock, J.E., Remillard, R.A. 2000, ApJ 531 956
 Nowak, M., Heinz, S., Begelman, M. 2002, ApJ 573 778
 Rutledge, R.E., Bildsten, L., Brown, E.F., Pavlov, G.G., Zavlin, V.E. 2001, ApJ 551 921
 Rutledge, R.E., Bildsten, L., Brown, E.F., Pavlov, G.G., Zavlin, V.E., 2002, ApJ 577 346
 Shahbaz, T., Naylor, T., Charles, P.A. 1993, MNRAS 265 655
 Tavani, M., Arons, J. 1997, ApJ 477 439
 Turner, M. et al., 2001, A&A 365 L27
 Wagner, R.M., Starrfield, S.G., Hjellming, R.M., Howell, S.B., Kreidl, T.J. 1994, ApJ 429 L25
 Wilms, J., Allen, A., McCray, R. 2000, ApJ 542 914
 Zurita, C., Casares, J., Shahbaz, T. 2003, ApJ 582 369

TABLE 1
SPECTRAL MODELS FOR THE ENTIRE XMM-NEWTON OBSERVATION.

Model	N_H (10^{20} cm $^{-2}$)	kT (eV)	Photon index	χ^2_{red} (d.o.f.)	n.h.p.
Hydrogen	8.3 ± 3.5	85 ± 3	1.56 ± 0.09	1.07 (518)	12.0%
Solar	11.1 ± 1.5	> 14	3.41 ± 0.08	2.88 (518)	0.0%
Iron	4.5 ± 1.0	< 273	2.79 ± 0.09	2.23 (518)	0.0%
Disk BB	7.3 ± 2.2	219 ± 13	1.73 ± 0.13	1.31 (518)	0.0%
Blackbody	< 1.4	186 ± 5	1.64 ± 0.09	1.06 (518)	16.1%

TABLE 2
STANDARD SPECTRAL MODELS FITS FOR THE HIGH AND LOW COUNT RATE INTERVAL.

Model	N_H (10^{20} cm $^{-2}$)	kT (eV)	Photon index (hard component)	χ^2_{red} (d.o.f.)	N.h.p.
Low	6.0 ± 2.9	87 ± 1	1.53 ± 0.17 (40%)	2.60 (450)	0%
Medium					
High					
Low	15.1 ± 3.6	78 ± 9	1.60 ± 0.14 (35%)	1.51 (448)	0%
Medium	8.9 ± 4.3				
High	4.4 ± 3.4				
Low	5.1 ± 2.6	86 ± 7	1.47 ± 0.13 (46%)	1.02 (446)	37%
Medium	4.6 ± 2.6	91 ± 5			
High	6.0 ± 2.1	99 ± 7			
Low	9.6 ± 4.6	85 ± 6	1.32 ± 0.19 (33%)	1.03 (444)	34%
Medium	5.4 ± 3.7		1.62 ± 0.16 (42%)		
High	4.6 ± 3.8		2.11 ± 0.20 (53%)		

Note. — The emitting radius of the neutron star atmosphere component has been constrained to be the same in all the three observations. In the case of a varying neutron star atmosphere model the radius is 9.7 ± 2.4 km (intrinsic radii), whereas for a varying power law we have a radius of 11.5 ± 6.0 km.

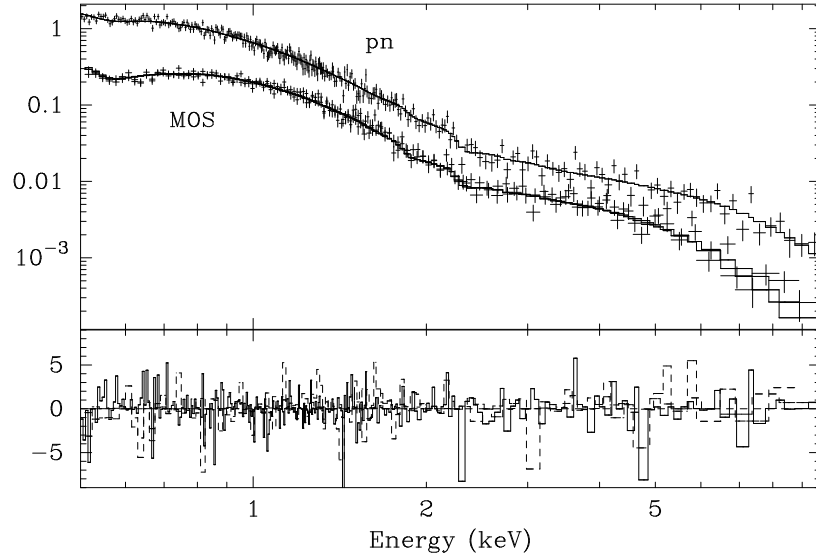


FIG. 1.— MOS and pn spectrum of Cen X-4 in the 0.5–10 keV range with the best fit model (absorbed neutron star atmosphere plus power law) overlaid. In the lower panel the differences between data and model in terms of χ^2 . Dashed lines in the lower panel refer to MOS data.

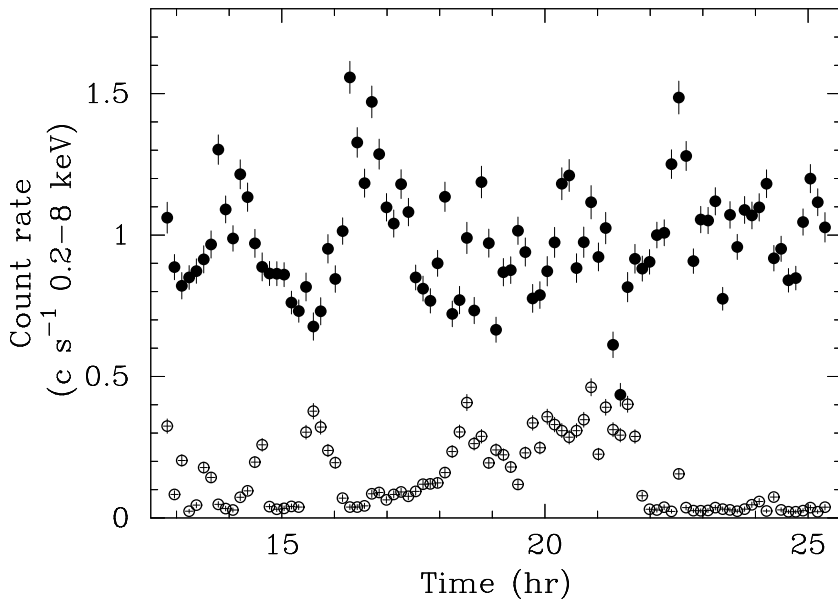


FIG. 2.— Background subtracted 0.2–8 keV pn light curve of Cen X-4. The bin size is 500 s. Open dots represent the background light curve scaled to the source extraction area (which has been already subtracted in the light curve above).

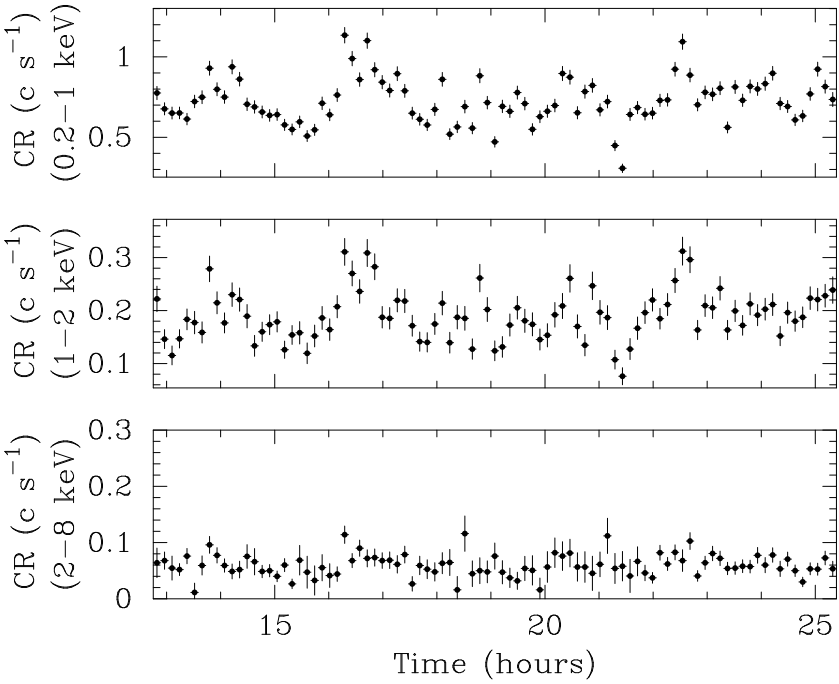


FIG. 3.— Background subtracted 0.2–8 keV pn light curve of Cen X-4 in three energy bands: 0.2–1 keV (upper panel); 1–2 keV (middle panel) and 2–8 keV (lower panel). The bin size is 500 s.

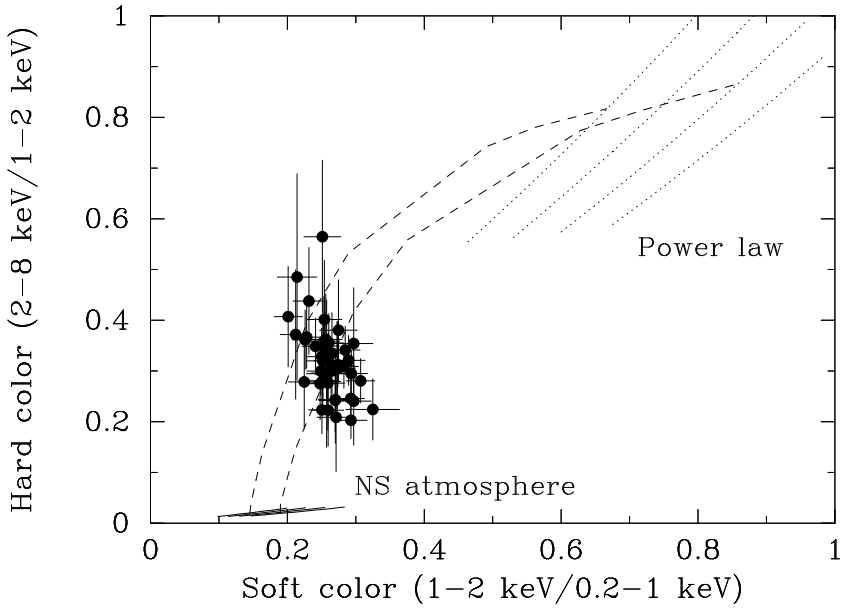


FIG. 4.— Color-color diagram of the pn background subtracted light curve. The soft color is defined as the ratio of the counts in the 0.2–1 keV to 1–2 keV, the hard color as the ratio of the counts in the 2–8 keV to 1–2 keV. On top of this we depict hardness ratios for an absorbed power law model (with photon index from 1.2 to 2) and an absorbed neutron star atmosphere model (with temperatures from 70 to 100 eV) for different values of column densities ($3, 5, 7, 9 \times 10^{20} \text{ cm}^{-2}$, dotted lines). Two different (dashed) curves connect the single component models with increasing contribution from the two for column densities of 5 and $9 \times 10^{20} \text{ cm}^{-2}$.